The complexometric behavior of selected aroyl-S,N-ketene acetals shows that they are more than AIEgens

Lukas Biesen & Thomas J. J. Müller

Article - Version of Record

scientific reports

Check for updates

OPEN

The complexometric behavior of selected aroyl-*S*,*N*-ketene acetals shows that they are more than AIEgens

Lukas Biesen[1,2] & Thomas J. J. Müller[1]✉

Using the established synthetic methods, aroyl-*S*,*N*-ketene acetals and subsequent bi- and multichromophores can be readily synthesized. Aside from pronounced AIE (aggregation induced emission) properties, these selected examples possess distinct complexometric behavior for various metals purely based on the underlying structural motifs. This affects the fluorescence properties of the materials which can be readily exploited for metal ion detection and for the formation of different metal-aroyl-*S*,*N*-ketene acetal complexes that were confirmed by Job plot analysis. In particular, gold(I), iron(III), and ruthenium (III) ions reveal complexation enhanced or quenched emission. For most dyes, weakly coodinating complexes were observed, only in case of a phenanthroline aroyl-*S*,*N*-ketene acetal multichromophore, measurements indicate the formation of a strongly coordinating complex. For this multichromophore, the complexation results in a loss of fluorescence intensity whereas for dimethylamino-aroyl-*S*,*N*-ketene acetals and bipyridine bichromophores, the observed quantum yield is nearly tripled upon complexation. Even if no stable complexes are formed, changes in absorption and emission properties allow for a simple ion detection.

Small traces of metal ions are ubiquitous. They can be found in nearly everything, i.e. in potable water, in nutriments, and in solvents for chemical reactions[1,2]. And while specific metals are essential for our survival and our health[3,4], others pose a great danger due to high toxicity[5–7]. Yet, even essential metal ions can be as well toxic at elevated concentration[3,8–10]. Therefore, the precise detection of metal ions in analytics[11] as well as in therapy and diagnostics[12] is of utmost importance. The requirements are quite rigorous with respect to detection limit and selectivity[13,14]. Electrochemistry and engineering provided various devices to ensure high quality metal ion sensing[15–19]. Another discipline, which garnered lots of attention regarding metal ion sensing, is dye chemistry in which the presence of metal ions leads to a change of photophysical properties, thus, resulting in a preferential optical readout[14,20–27]. While the range of suitable dyes for metal ion sensing is broad, a common ground for the overwhelming majority are ligands with heteroatoms, as they often act as sites of coordination[28–33]. The modes of action for these metal ion sensors are as manifolded as their structural motifs and span from metal organic frameworks[34–36] to classic fluorescent probes[37–40] up to doped materials[20,41] and carbon[42–44] and quantum dots[45,46]. Due to the phenomenal impact of aggregation induced emission (AIE), AIEgens have also been implemented as promising metal sensors due to their remarkable fluorescence light up under specific circumstances[47–52].

Since 2020, aroyl-*S*,*N*-ketene acetals quite successfully entered the stage of novel and exciting AIEgens due to their high versatility and their unusual AIE properties based on the presence of benzyl moieties[53,54]. By various expansions, the bouquet of photophysical properties for this class of compounds has been vastly expanded by exploiting the full potential of synthetic organic chemistry[53,55–59]. Aside from AIE, solid-state and dual emission, solvatochromism, and halochromism properties were unveiled for this class of compound[53,60]. One fact that has been overlooked for aroyl-*S*,*N*-ketene acetal based AIEgens so far, is the dyes' behavior in the presence of metal ions. Due to various heteroatoms embedded into the molecular structure, the assumption of complexing behavior seemed feasible. Benzothiazole derivatives are applied in *N*-heterocyclic carbene ligands (NHCs), especially *N*-allyl-substituted derivatives have been successfully used in these respects[61–63]. Furthermore, a 2,5-bis[3-benzyl-2-methylbenzothiazole] croconaine derivative could be used as a highly sensitive and selective sensor for the detection of iron(III) ions with the naked eye[64]. Due to an identical distance between carbonyl oxygen

[1]Heinrich-Heine-Universität Düsseldorf, Math.-Nat. Fakultät, Institut für Organische Chemie und Makromolekulare Chemie, Universitätsstraße 1, 40225 Düsseldorf, Germany. [2]School of Chemistry, Joseph Black Building, University of Glasgow, Glasgow G12 8QQ, UK. ✉email: ThomasJJ.Mueller@hhu.de

and sulfur atom of the benzothiazole of the 2,5-bis[3-benzyl-2-methylbenzothiazole] croconaine derivative in comparison to the structural motif of the aroyl-*S*,*N*-ketene acetals, these complexing properties inspired to perform comparable complexometric studies for the aroyl-*S*,*N*-ketene acetal class of compounds. Due to the emission properties of the dimethylamino-substituted aroyl-*S*,*N*-ketene acetals and their derivates, we chose to make them the centerpiece of the present complexometric investigations.

Results and discussion

Synthesis

First generation dimethylamino aroyl-*S*,*N*-ketene acetals **3a**[54] and **3b**[54] can be easily obtained via an addition–elimination sequence, starting from the respective acid chloride and a benzothiazolium salt **2** using diisopropylethylamine as a base in very good yields (Fig. 1A)[54].

Another fluorescent aroyl-*S*,*N*-ketene acetal based material, which might be suitable for complexometric studies, are triphenylamine aroyl-*S*,*N*-ketene acetals that are accessible via a one-pot procedure, where the addition–elimination procedure is followed en route by a Suzuki coupling with triarylamine boronate **4a**[65] to give the respective bichromophore **5a**[57] in a yield of 66% (Fig. 1B)[57]. Similarly, a single step Suzuki reaction of dimethylamino aroyl-*S*,*N*-ketene acetal **3a** and bipyridine boronic acid ester **4b** leads to the formation of the respective bipyridine bichromophore **5b** in excellent yield (Fig. 1C).

By using an excess of dimethylamino aroyl-*S*,*N*-ketene acetal **3a** implemented in a Masuda borylation-Suzuki coupling (MBSC)[66] sequence with dibrominated 1,10-phenanthroline as a coupling partner, it is possible to generate the 1,10-phenanthroline bridged dimethylamino aroyl-*S*,*N*-ketene acetal multichromophore **5c** in moderate yield (Fig. 1D)[56].

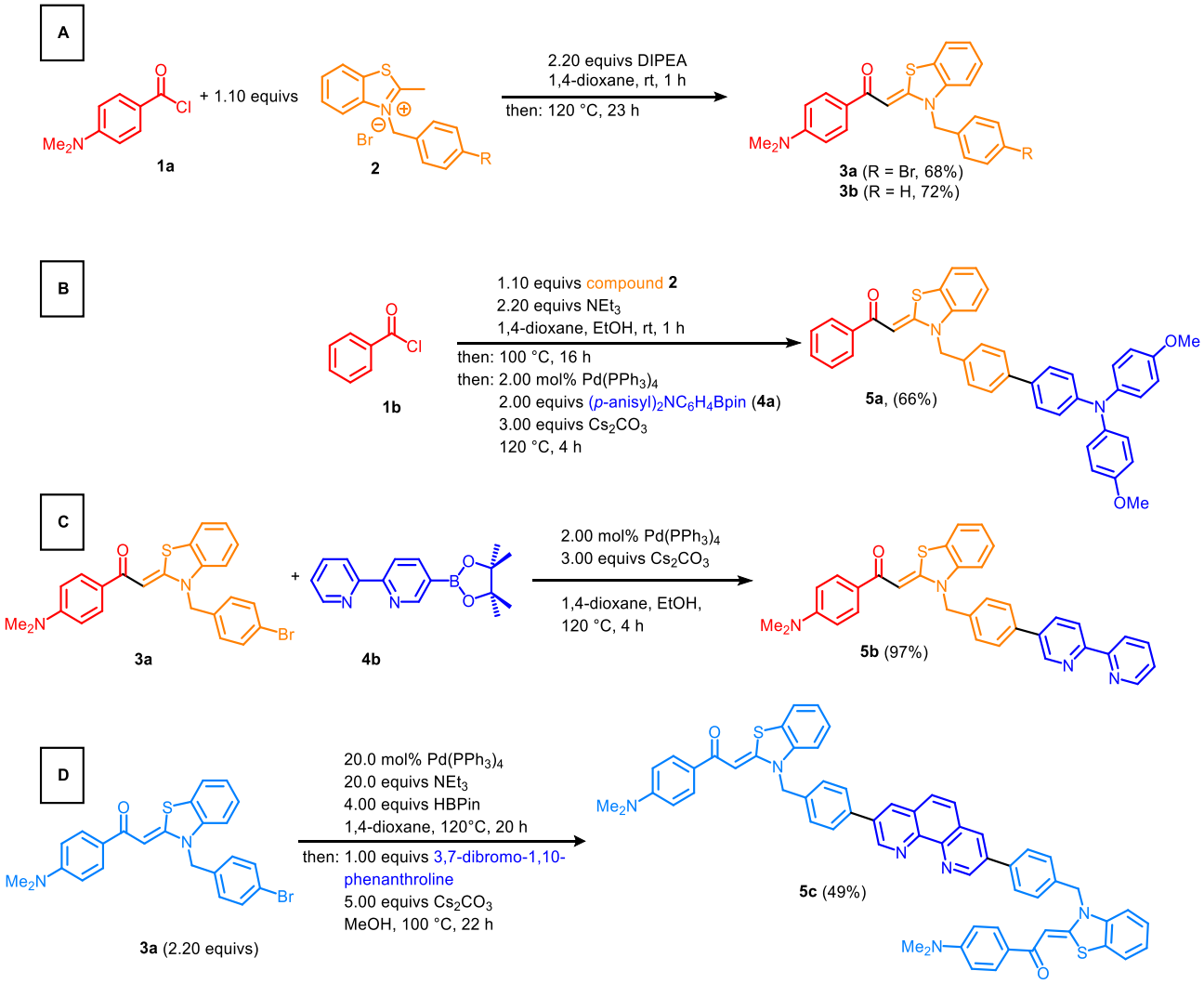

Figure 1. Addition–elimination reaction for the generation of dimethylamino substituted aroyl-*S*,*N*-ketene acetals **3a** and **b** (**A**), Consecutive three-component condensation-Suzuki coupling synthesis of aroyl-*S*,*N*-ketene acetal bichromophore **5a** (**B**), Suzuki coupling synthesis of dimethylamino aroyl-*S*,*N*-ketene acetal bipyridine bichromophore **5b** (**C**), MBSC synthesis of 1,10-phenanthroline bridged trichromophore **5c** (**D**).

Photophysical properties

The photophysical properties of the investigated series of dyes in ethanol are mostly determined by the aroyl-*S*,*N*-ketene acetal moiety. As most of the dyes comprise of dimethylamino aroyl-*S*,*N*-ketene acetals, for compounds **3a**, **3b**, and **5b** show nearly identical absorption properties with absorption maxima of 404 nm, only bichromophore **5a** and multichromophore **5c** deviate from this behavior due to the secondary chromophores of triphenylamine and 1,10-phenanthroline, resulting in absorption maxima of 373 nm. Regarding the luminescence in ethanol, the emission properties are determined by the dimethylamino aroyl-*S*,*N*-ketene acetal units due to their intense emission at 455 nm and fluorescence quantum yields Φ_f of around 0.20. Only bichromophore **5a** fluoresces at 447 nm as the unsubstituted aroyl-*S*,*N*-ketene acetal **3c** does not fluoresce in solution[54]. Therefore, the properties are determined by the secondary triphenylamine chromophore (Fig. 2A). The solid-state emission exhibits a greater range, which is determined by both the aroyl-*S*,*N*-ketene acetal and the secondary chromophore. The most blue shifted derivative is the triphenylamine bichromophore **5a** with a solid-state emission maximum of 500 nm, whereas the most bathochromically shifted emission maxima occur for both the dimethylamino bipyridine bichromophore **5b** and the brominated dimethylamino aroyl-*S*,*N*-ketene acetal **3a** with $\lambda_{max,em}$ = 604 nm (Fig. 2B) (for full details of photophysical properties, see SI chpt.6).

As aggregation induced emission is normally a prime feature for aroyl-*S*,*N*-ketene acetals, we could only observe partial aggregation caused quenching effect in conjunction with a bathochromic shift of the emission maximum, which can be unequivocally attributed to the dimethylamino substituted aroyl-*S*,*N*-ketene acetal core (for details, see SI, chpt. 7).

Complexometric studies

The standard method for determining complex stoichiometry is to use the method of continuous variation that is shown in the Job plot[67,68]. This assumes a constant total volume and concentration of all components involved in the equilibrium. The continuous variation of the ratios of metal salt and ligand concentration allows the complex stoichiometry to be determined via the change in the physical quantity under consideration. For the required Job plot, the variable photophysical quantity must be plotted against the mole fraction. It should also be noted that free binding sites in the complex can be occupied by solvent molecules if coordinating solvents are present[67,68].

A series of qualitative tests were carried out for the dimethylamino-substituted compound **3b** by adding small amounts of various metal salts to a solution of the dye in ethanol and observing with the naked eye the influence this has on the absorption and emission properties of the dissolved chromophore. As expected, gold(I), iron(III), and ruthenium(III) salts were identified as potential candidates for complexometric studies. We screened for a variety of the most common metal salts of both transition metals and metals like sodium, potassium, magnesium, calcium, aluminum, silver, gold, iron, tin, nickel, platin, zinc and scandium ions in order to cover up the widest range possible of metals that are most commonly used and can be called ubiquitous.

First, the complexation properties of the aroyl-*S*,*N*-ketene acetal **3b** with gold(I) iodide are investigated (Fig. 3). This initially revealed an interesting effect when looking at the emission properties during complexation: there is a continuous increase in the emission intensity and an associated increase from Φ_f = 0.20 in the absence of a metal salt to Φ_f = 0.55 in presence of AuI (2.43 equivs) (Fig. 3B). A further increase of the amount of metal salt causes a slight decrease in the emission intensity.

The formation of difference spectra before and after addition of the metal salt reveals the most pronounced change for the absorption maximum at a wavelength of 271.5 nm (Fig. 3A). The corresponding absorbance values of the difference spectra at this maximum are plotted against the corresponding mole fraction χ of the ligand

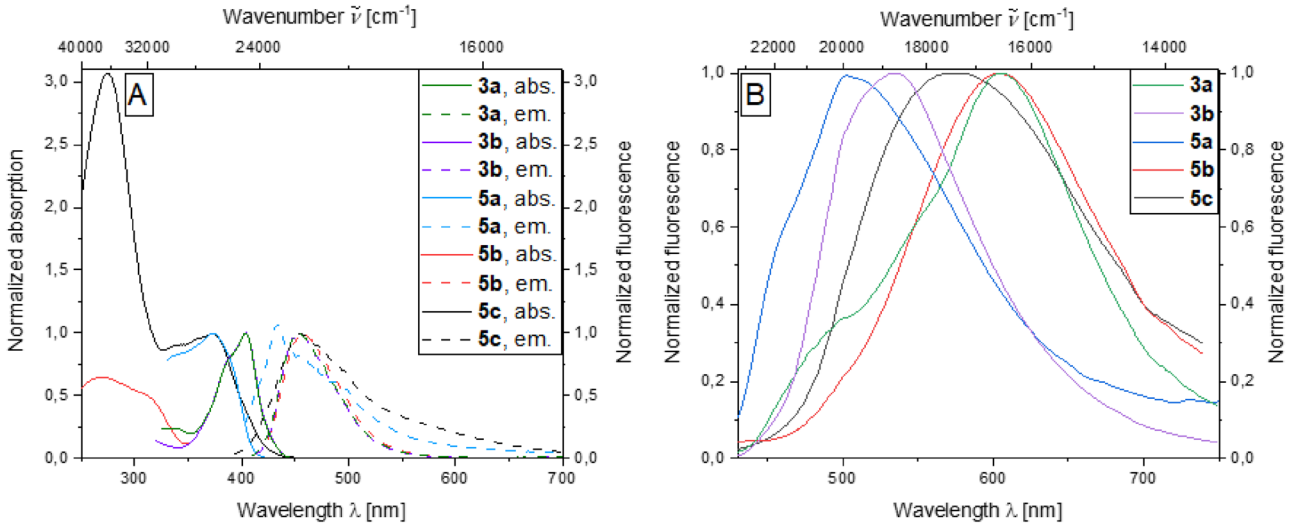

Figure 2. Normalized absorption and emission spectra in ethanol (T = 298 K, c(abs) = 10^{-5} M, c(em) = 10^{-7} M, $\lambda_{exc} = \lambda_{max,abs}$) (**A**) and normalized solid-state emission spectra and solid-state fluorescence colors (**B**) of aroyl-*S*,*N*-ketene acetals **3** and **5** (λ_{exc} = 365 nm; $\lambda_{exc} = \lambda_{max(abs)}$).

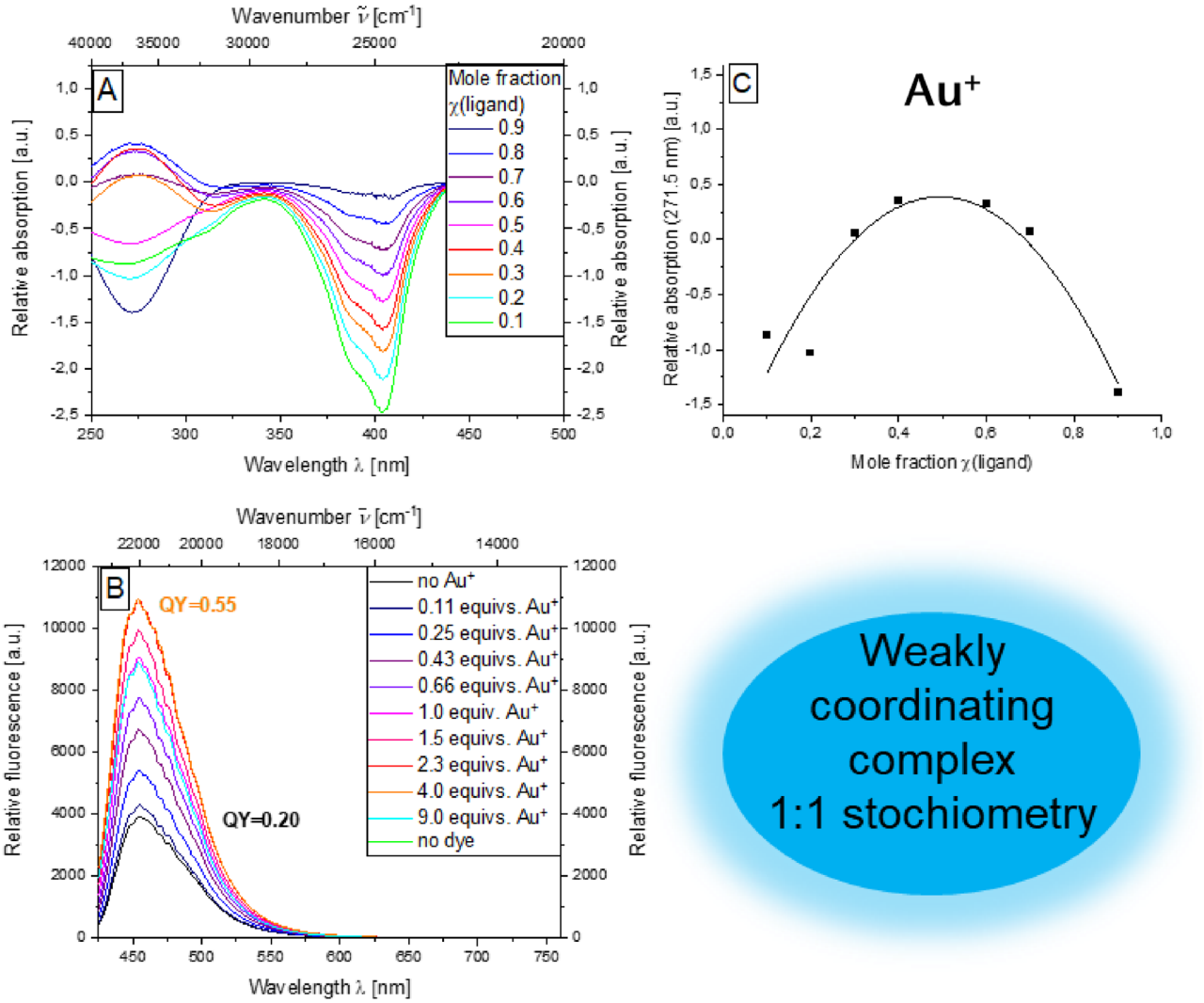

Figure 3. Absorption difference spectra of compound **3b** at different mole fractions of the ligand dye in the presence of AuI (recorded in ethanol; c(**3b**) = 10^{-5} M, c(metal salt) = 10^{-5} M, T = 298 K) (**A**), emission spectra of compound **3b** with increasing amount AuI (c(**3b**) = 10^{-7} M, c(metal salt) = 10^{-7} M, T = 298 K, λ_{exc} = 404 nm) (**B**), Job plot of the mole fraction of the ligand against the relative absorption at 271.5 nm (**C**).

gives the respective Job plot that is fitted by a quadratic correlation with $f(\chi) = -10.308 - \chi^2 + 10.190 - \chi - 2.1$ 29 and an excellent correlation factor ($R^2 = 0.96$). The paraboloid course of the function and the maximum of the negative parabola is localized at a mole fraction of $\chi = 0.5$ indicates a weakly coordinating complex of aroyl-*S*,*N*-ketene acetal **3b** and Au^+ ion. (Fig. 3C).

A similar behavior could be observed for both iron and ruthenium salts. Since the Fe^{3+}-complexing properties of a benzothiazole croconaine derivative[64] served as the motivation for investigating the complexing properties of aroyl-*S*,*N*-ketene acetals, aroyl-*S*,*N*-ketene acetals are intriguing to be also checked for complexation with Fe^{3+} ions. Iron(III) chloride is used as the metal salt for this purpose, and complexing properties of the aroyl-*S*,*N*-ketene acetals are indeed revealed. Once again, there is a clear increase in fluorescence intensity due to complexation Fe^{3+} ions to Φ_f = 0.59 (see SI, Fig. S9B) and for Ru^{3+} ions to 0.57 (see SI, Fig. S10B). Both, iron ($f(\chi) = -1$ 2.646 $- \chi^2 + 10.991 - \chi - 1.152$) and ruthenium ($f(\chi) = -0.499 - \chi^2 + 0.597 - \chi - 1.521$) show good correlations with their respective fits of 0.93 and 0.86. For Fe^{3+}-ions, a weakly coordinating 1:1 complex can be observed (see SI Fig. S9) while for Ru^{3+}-ions, a weak complex with a 1:2 stoichiometry seems to be rational (see SI Fig. S10).

Several possible explanations for the observed fluorescence enhancements upon ligation can be given. The enhancement may result from ion-induced changes in the geometry or flexibility of the ligand. Other possibilities include chelation-induced changes of the relative energetic positions of different states, which shut off deactivation pathways as well as surpassing radiationless deactivation pathways via torsional motions which may be a viable explanation for aroyl-*S*,*N*-ketene acetals. The determination of the mechanism behind these fluorescence enhancements have been studied for more than 20 years and are still basis of currently ongoing investigations[69–71].

Theoretically, various complexation modes of the dimethylamino-aroyl-*S*,*N*-ketene acetal **3b** are conceivable. Coordination can either take place via the lone pairs of the dimethylamino group, the carbonyl oxygen, the

sulfur atom of the benzothiazole or simultaneously via the carbonyl oxygen and the sulfur atom, i.e. by chelation. Previous studies suggested coordination via carbonyl oxygen and benzothiazole sulfur for 1:1 stoichiometry of comparable ligand systems[64]. In the case of the ruthenium complex, it can therefore be assumed that the ruthenium can be coordinated via carbonyl oxygen and benzothiazole sulfur as well as via the dimethylamino unit[72–74].

For bichromophore system **5a**, a pronounced effect of fluorescence quenching can be observed with the addition of iron(III) chloride; a weak effect can also be observed with regard to absorption spectroscopy.

In contrast to the complexometric studies of **3b** (Fig. 4A), a decrease in fluorescence intensity of the bichromophore **5a** can be observed with increasing mole fraction until the emission is finally extinguished (Fig. 4B). One possibility for the fluorescence quenching are competing electron transfer processes: the ligand is excited and Fe(III) is thus reduced to Fe(II) by the excited ligand. Another possible explanation addresses the effect of the comparable quenching behavior during protonation which we reported earlier for triphenylamine bichromophores[57]. The fluorescence can be attributed to the emissive triphenylamine secondary chromophore. However, an energy transfer to the aroyl-*S*,*N*-ketene acetal system can be assumed[57]. The systemic change in the molecule takes place at the aroyl-*S*,*N*-ketene acetal motif, which is responsible for the fluorescence quenching, and not at the triphenylamine, which is affected neither by complexation nor protonation.

The most obvious assumption of the complexation site is the sulfur and oxygen atoms of the aroyl unit and the benzothiazole unit.

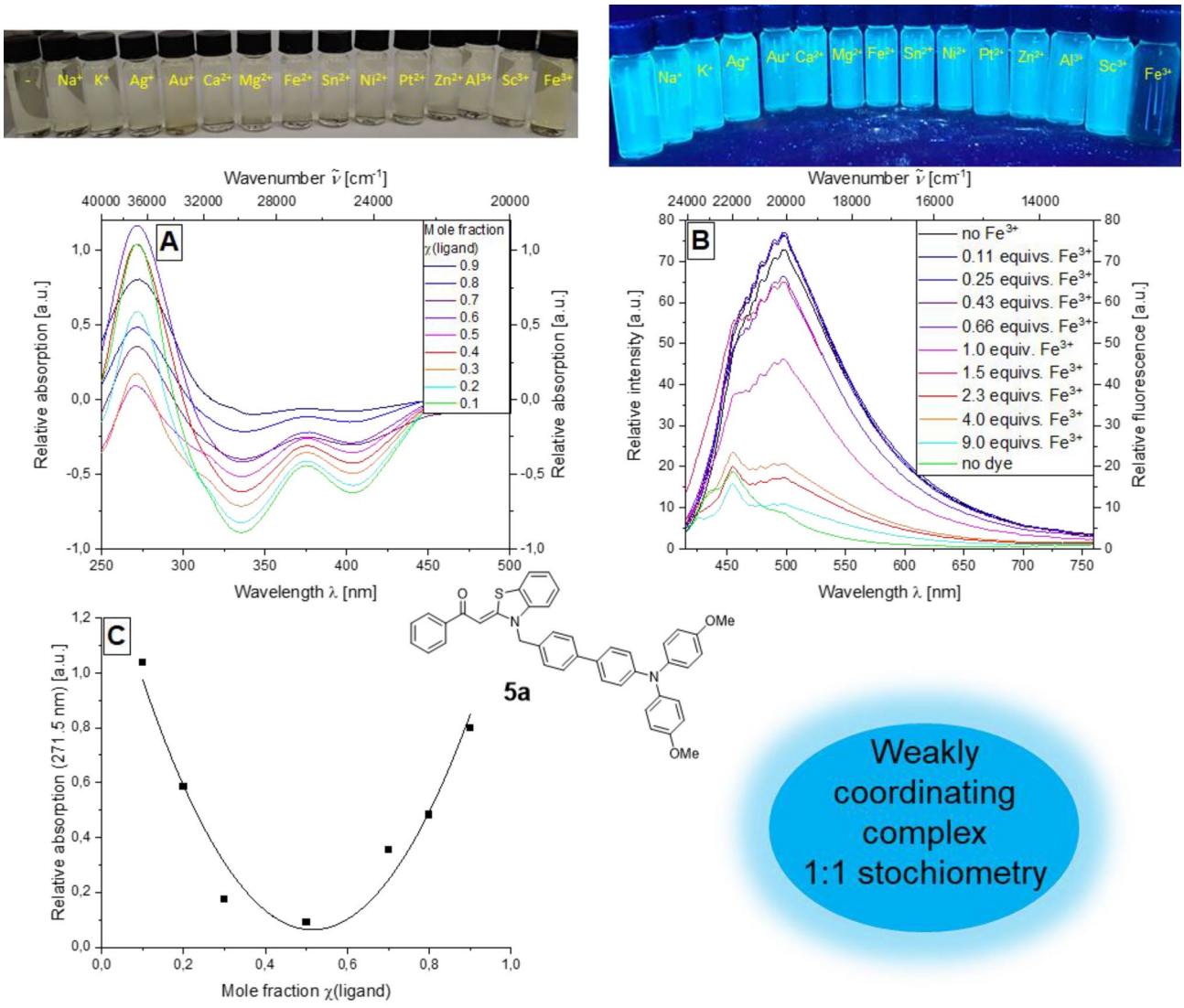

Figure 4. Top: apparent perception of the properties of **5a** when different metal salts are added in daylight (left) and under UV light (right); middle: absorption difference spectra of compound **5a** at different mole fractions of the ligand dye in the presence of $FeCl_3$ (recorded in ethanol; $c(\mathbf{5a}) = 10^{-5}$ M, $c(FeCl_3) = 10^{-5}$ M, T = 298 K) (**A**), Emission spectra of compound **5a** with increasing amount of $FeCl_3$ ($c(\mathbf{5a}) = 10^{-7}$ M, $c(FeCl_3) = 10^{-7}$ M, T = 298 K, $\lambda_{exc} = 373$ nm) (**B**); bottom: Job plot of the mole fraction of the ligand against the relative absorption at 271.5 nm (**C**).

The determination of the difference spectra showed that the most pronounced effect could be observed for the absorption maximum at 271.5 nm. Therefore, this maximum was selected for the creation of the corresponding Job plot.

Plotting the mole fraction of the ligand against the relative absorbance at 271.5 nm results in a paraboloid curve, which indicates a weakly coordinating complex. The position of the maximum at $\chi = 0.5$ indicates a 1:1 stoichiometry of the fluorescence quenching complex (Fig. 4C).

As for compound **3b**, it was also possible to proceed for the combination of ruthenium(III) chloride and bichromophore **5b**. With regard to the emission intensity, the intensity can also be increased by adding the dissolved metal salt. At the same time, the fluorescence quantum yield can be more than doubled from $\Phi_f = 0.20$ to 0.45 (Fig. 5B). In the case of ruthenium(III) chloride, the difference spectra reveal that the absorption maximum at 348.5 nm is most suitable for investigation using Job plot analysis (Fig. 5A). The Job plot of the mole fraction of the ligand χ against the relative absorbance at 348.5 nm provides a parabola that is highly correlated with the individual measurement points, so that a weakly coordinating complex can also be detected in this case. The maximum of this parabola was at $\chi = 0.5$, meaning that a 1:1 stoichiometry of the ruthenium dye complex can be assumed (Fig. 5C).

Although no complex formation can be observed for other metal ions, the presence of various metal ions nevertheless has an obvious influence on the absorption and emission properties of bichromophore **5b** dissolved in ethanol during qualitative tests. For this purpose, low concentrations of both the bichromophore **5b** and the respective metal salt of $c = 10^{-5}$ M for absorption and $c = 10^{-7}$ M for emission are used. While an absorption maximum at 315 nm can be observed in the absence of a metal salt, this maximum disappears in the presence of metal ions. For the presence of gold ions, the maximum mentioned appears at 271.5 nm. The addition of ruthenium(III) chloride causes a bathochromic shift of the long wavelength absorption maximum. Furthermore,

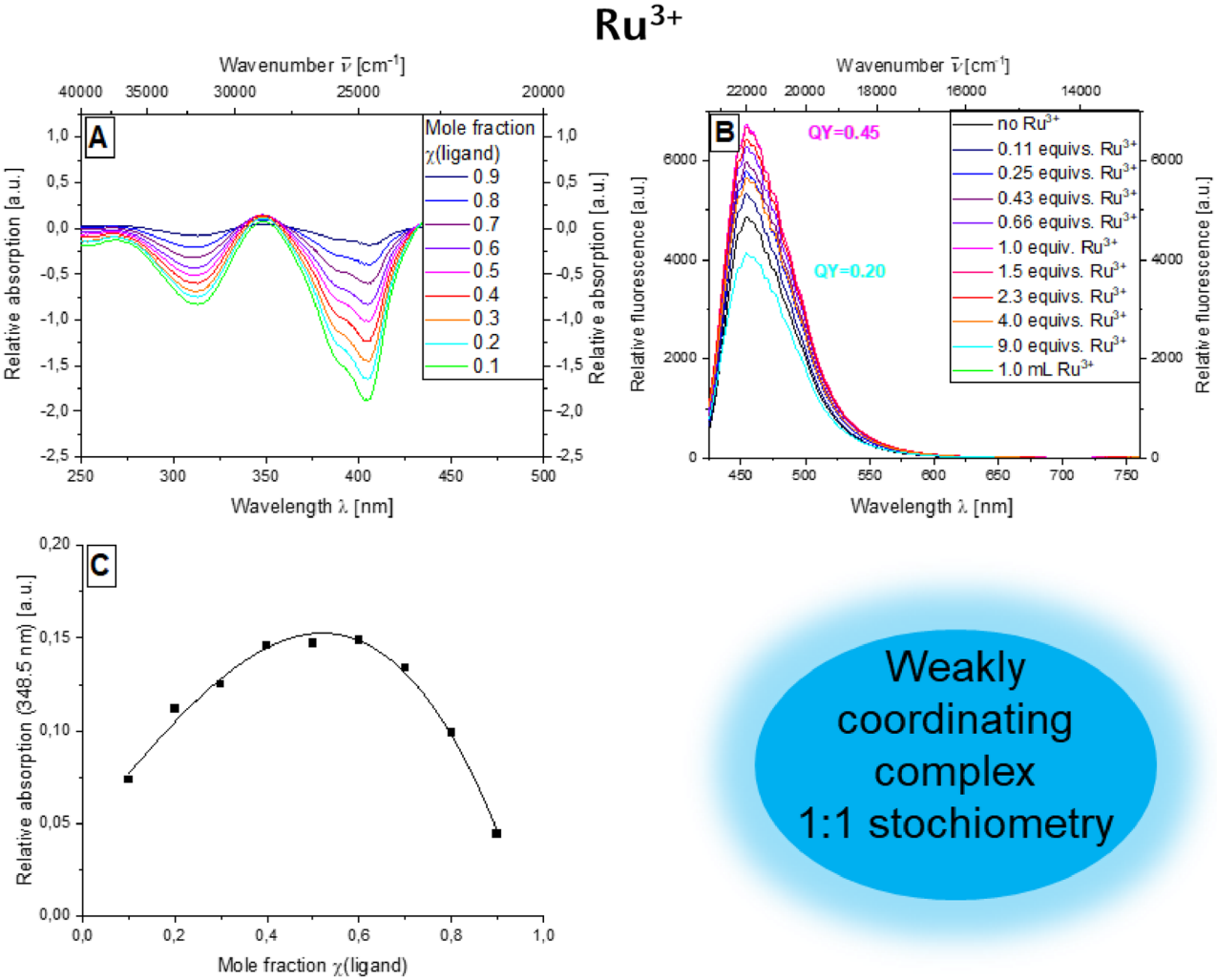

Figure 5. Absorption difference spectra of compound **5b** at different mole fractions of the ligand dye in the presence of $RuCl_3$ (recorded in ethanol; $c(\mathbf{5b}) = 10^{-5}$ M, $c(RuCl_3) = 10^{-5}$ M, T = 298 K) (**A**), emission spectra of compound **5b** with increasing amount of $RuCl_3$ ($c(\mathbf{5b}) = 10^{-7}$ M, $c(RuCl_3) = 10^{-7}$ M, T = 298 K, $\lambda_{exc} = 404$ nm) (**B**), Job plot of the mole fraction of the ligand against the relative absorption at 348.5 nm (**C**).

the addition of iron(II) sulfate, iron(III) chloride and aluminum(III) chloride results in a longer wavelength absorption maximum which can be ascribed to the long wavelength metal to ligand charge transfer bands. This absorption maximum occurs for Fe^{2+} ions at 495 nm, for trivalent iron ions this maximum occurs with increased intensity bathochromically shifted to 505 nm.

This effect can be observed even more strongly in the presence of Al^{3+} ions, where the maximum occurs at 513 nm (Fig. 6A). With regard to the emission, an effect due to the presence of metal ions can also be demonstrated. Without the addition of metal salts, the emission maximum occurs at 447 nm. In presence of Pt^{2+} ions and Ag^{+} ions, a bathochromic shift of the emission maximum to 497 and 502 nm, respectively, can be observed. The most significant effect occurred in the presence of Al^{3+} ions. The respective emission maximum can be detected here at 520 nm (Fig. 6B).

In comparison to the other systems **3b**, **5a**, and **5b** investigated, a strongly altered emission behavior of the bis(dimethylamino-aroyl-*S*,*N*-keteneacetal)-1,10-phenanthroline system **5c** can be observed. So far, the presence of the metal salts has led to a significant increase in the fluorescence quantum yield Φ_f. In the case of the presence of the phenanthroline linker, the pronounced fluorescence quantum yield of the dimethylamino-aroyl-*S*,*N*-ketene acetals is already significantly reduced to 0.04. In addition, the fluorescence quantum yield Φ_f decreases significantly with increasing mole fraction of the gold(I) iodide, with the greatest drop in emissivity already occurring upon addition of 0.11 equivs of gold(I) iodide. The further decrease in the fluorescence quantum yield Φ_f with increasing mole fraction is almost linear (see SI, Fig. S15B).

The formation of the corresponding difference spectra reveals the greatest change for an absorption wavelength of 449 nm, so that these respective absorption values of the difference spectra at different mole fractions of the ligand could be used for the analysis using a Job plot (Fig. 7, top A). It is possible to fit the course of the complexation behavior by a quadratic function, so that formation of a weakly coordinating complex can be assumed. The maximum of the parabola is localized at a mole fraction of $\chi = 0.65$, so that a complex consisting of two Au^{+} ions and a molecule of the 1,10-phenanthroline system **5c** is formed (see SI, Fig. S15C).

In contrast to previously investigated systems, complexation of Fe^{2+} ions is observed in the case of derivative **5c**, such as complexation must be attributable to the 1,10-phenanthroline linker. It can be seen that quenching of the emission in the presence of the metal salt is a material property of derivative **5c**, since the initial fluorescence quantum yield Φ_f of 0.04 decreases significantly when the metal salt loading is increased (Fig. 7, top B).The difference spectra of compound **5c** reveal that the absorbance maximum at 400 nm is ideal for examination by Job plot analysis (Fig. 7, top right A). The plot of the absorbance at 400 nm against the mole fraction χ of the ligand again shows an almost parabolic curve and thus indicating a weakly coordinating complex. The position of the maximum at 0.6 suggests the formation of an iron-dye complex in a 1:2 stoichiometry (Fig. 7, top C).

Finally, the complexation behavior of the multichromophore **5c** with respect to iron(III) chloride (Fig. 7, bottom A) will be discussed. The quenching of the emission reaches its maximum with this metal salt and chromophore combination. After addition of 0.11 equivs of iron(III) chloride, almost complete quenching of the emission intensity is observed. The fluorescence quantum yield Φ_f decreases from 0.04 without any metal salt present to well below 0.01 upon the addition of the respective metal salt (Fig. 7, bottom B). With regard to the difference spectra obtained, the local maximum can be identified as suitable for Job plot analysis (Fig. 7, bottom A).The job plot of the mole fraction of the ligand χ against the relative absorbance at 362.5 nm yields a 7th degree function that is highly correlated with the individual measurement points and consists of two almost linear subsections, so that a strongly coordinating complex can be assumed in this case. At the same time, the position of the maximum of the 7th degree function at $\chi = 0.2$ indicates the formation of a complex with a 5:1

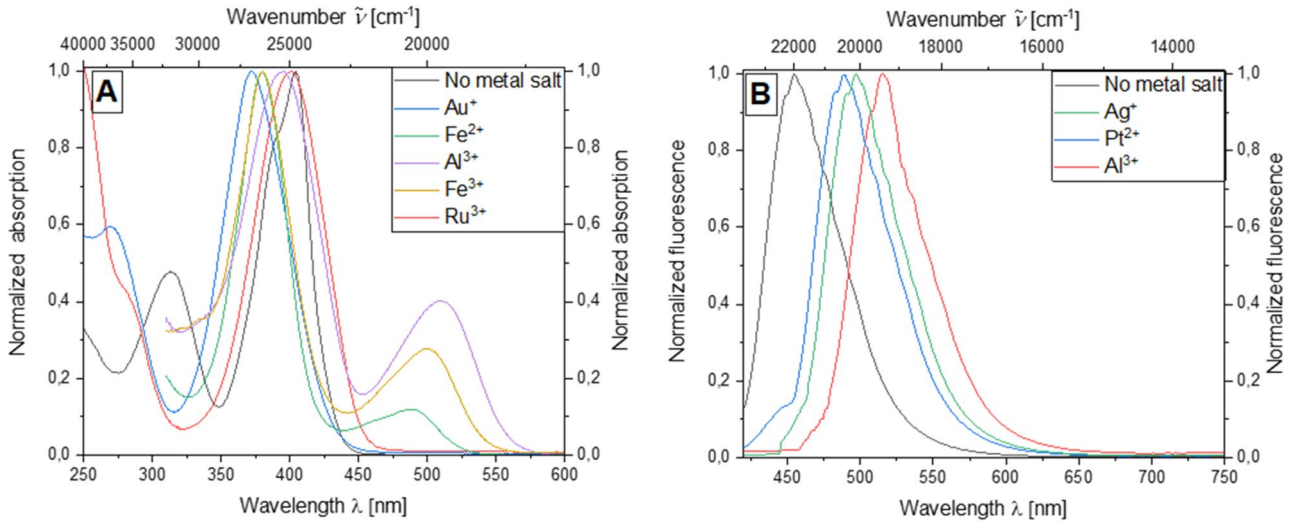

Figure 6. Absorption spectra on addition of various metal salts in ethanol (c(**5b**) = 10^{-5} M, $c(M^{+}) = 10^{-5}$ M, T = 298 K) (**A**) and emission spectra of compound **5b** on addition of various metal salts in ethanol (c(**5b**) = 10^{-7} M, $c(M^{+}) = 10^{-7}$ M, T = 298 K, λ_{exc} = 404 nm).

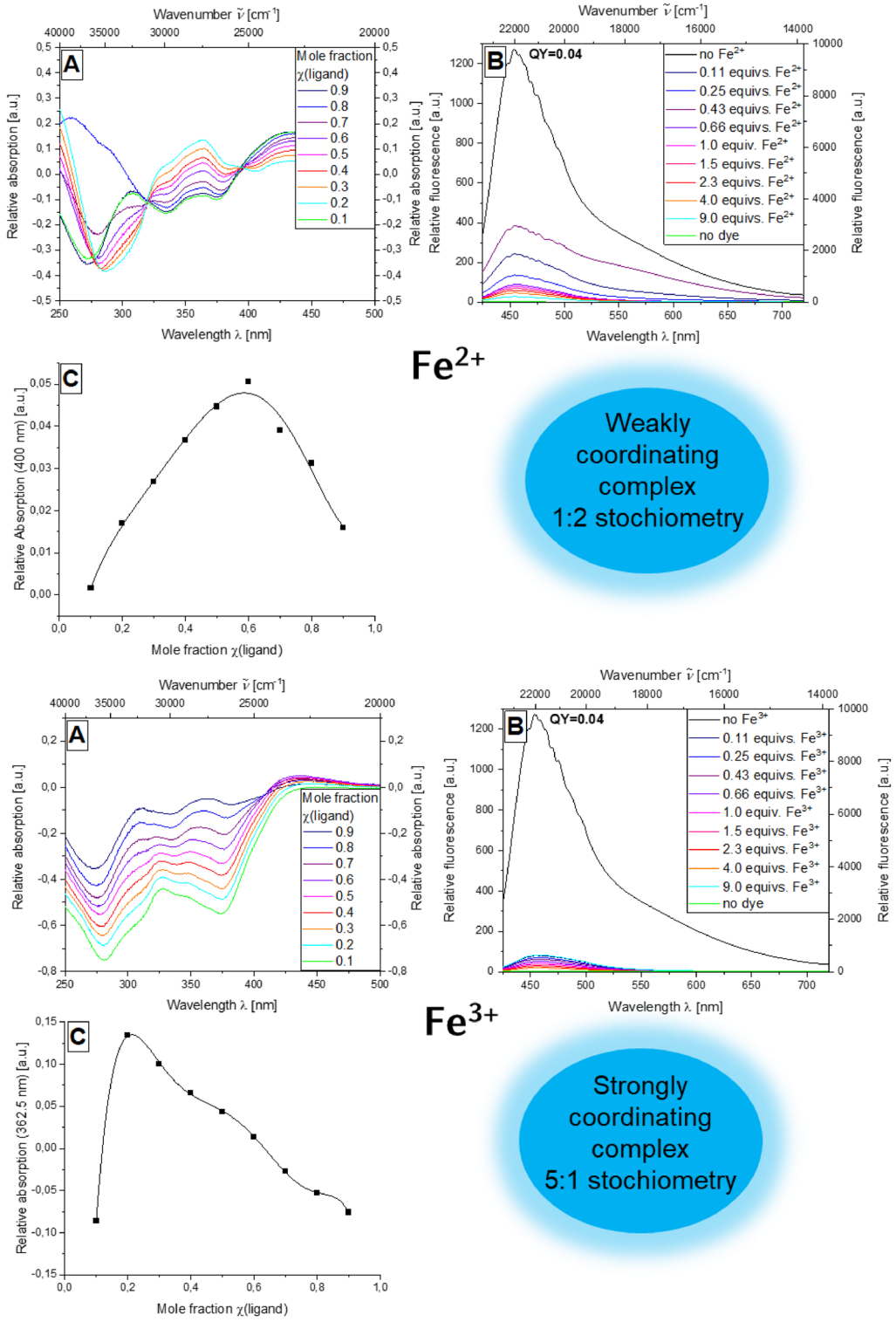

Figure 7. Absorption difference spectra of compound **5c** at different mole fractions of the ligand dye in the presence of $FeSO_4$ (top) and $FeCl_3$ (bottom) (recorded in ethanol; c(**5c**) = 10^{-5} M, c(metal salt) = 10^{-5} M, T = 298 K) (**A**), emission spectra of compound **5c** with increasing amount $FeSO_4$ (top) and $FeCl_3$ (bottom) (c(**5c**) = 10^{-7} M, c(metal salt) = 10^{-7} M, T = 298 K, λ_{exc} = 404 nm) (**B**), Job plot of the mole fraction of the ligand against the relative absorption at 271.5 nm ($FeSO_4$, top) and ($FeCl_3$, bottom) (**C**).

stoichiometry consisting of five ligands and one Fe^{3+} ion[67,68]. This behavior can be interpreted that Fe^{3+} ions coordinate to both 1,10-phenanthroline and the dimethylamino aroyl-*S*,*N*-ketene acetals (Fig. 7, bottom C).

Even if no stable and observable metal dye complexes are formed, the presence of metal ions still have a considerable effect on both absorption and emission properties of dye **5c**. To quantify the influence of the presence of the metal ions, low concentrations of $c = 10^{-5}$ M of both the metal salt used and the bridged system **5c** were used for emission and concentrations of $c = 10^{-7}$ M were used. The intense absorption maximum at 274 nm disappears almost completely in the presence of various metal salts. For some metal salts, the absorption at 320 nm is only plotted, as interfering absorption effects of the metal salt solutions occur at higher energies. For platinum(II) salts and silver(I) iodide, the formation of an additional, energetically higher absorption maximum can be detected at 318 and 341 nm, respectively. The absorption maximum which can be ascribed to the aroyl-*S*,*N*-ketene acetal unit occurring at 373 nm in the absence of the metal salts occurs almost unchanged in the presence of Ag^+, Fe^{2+} and Al^{3+} ions (Fig. 8A).

A similarly distinct behavior can also be detected for the emission of system **5c** in the presence of various metal salts. In the absence of additives, the emission maximum in ethanol occurs at 455 nm. The emission is bathochromically shifted to 498 nm in the presence of Al^{3+} ions, resulting in a greenish fluorescence. For the presence of Ni^{2+} and Pt^{2+} ions, the emission maximum in solution can be observed at 531 nm, whereas the emission intensity is clearly different and by a factor of 10 lower for the presence of Ni^{2+} ions. Comparably, the emission maxima occur with the addition of Sn^{2+} and Zn^{2+} ions at 542 and 546 nm, respectively, with significantly broadened emission bands. The solution of chromophore **5c** luminesces most intensely in the presence of silver(I) ions. Two emission maxima can be observed here, at 549 and 602 nm. The presence of Ru^{3+} ions results in the most pronounced bathochromic shift of the emission maximum. The solution of the dye luminesces orange in ethanol with an emission maximum of 592 nm (Fig. 8B).

The discrepancy between the emission behavior of the derivatives **3a** and **5b** and the derivative **5c** and their spectroscopically detected metal complexes suggests that two fundamentally divergent binding modes of the metal complexes are operative. It can be concluded that for chromophores **3a** and **5b** a constructive influence of the metal ions is in effect as emission quenching by energy or electron transfer does not occur in these cases. The most likely sites of coordination are in this case either the dimethylamino functionality or the potentially chelating oxygen-sulfur unit of aroyl and benzothiazole. For dimethylamino aroyl-*S*,*N*-ketene acetals, it is reasonable to assume that complexation also occurs via the amino nitrogen. But, as with all anilines, both the Brønsted and Lewis basicity is reduced by the aromatic compound, and even more so by the p-conjugation to the carbonyl group. Therefore, the carbonyl group even becomes more electron-rich as a result. Ergo, chelation, also for thermodynamic reasons, enthalpic and entropic, should actually be the most likely modus operandi for these systems. This means that the presence of the metal salt can have a fluorogenic effect as seen by the increase in the fluorescence quantum yield Φ_f (Fig. 9, top)[23,75–77]. A possible explanation for this behavior lies in the metal ion-induced changes in the geometry and flexibility of the ligand as well as reducing the accessibility of deactivation pathways of certain functional groups. Especially in case of flexible ligands like bipyridine or equally flexible aroyl-*S*,*N*-ketene acetal, the chelation process suppresses radiationless deactivation via torsional motions[40].

The quenching of the emission in the presence of transition metal ions, as observed for **5c**, clearly indicates that energy or electron transfer processes, as described in the literature[78,79], lead to emission quenching. Decisive for such processes the corresponding metal must coordinate to the central 1,10-phenanthroline, which has been shown to act as a quencher[80,81]. Therefore, it can be assumed that a quenching energy transfer (EnT) process from

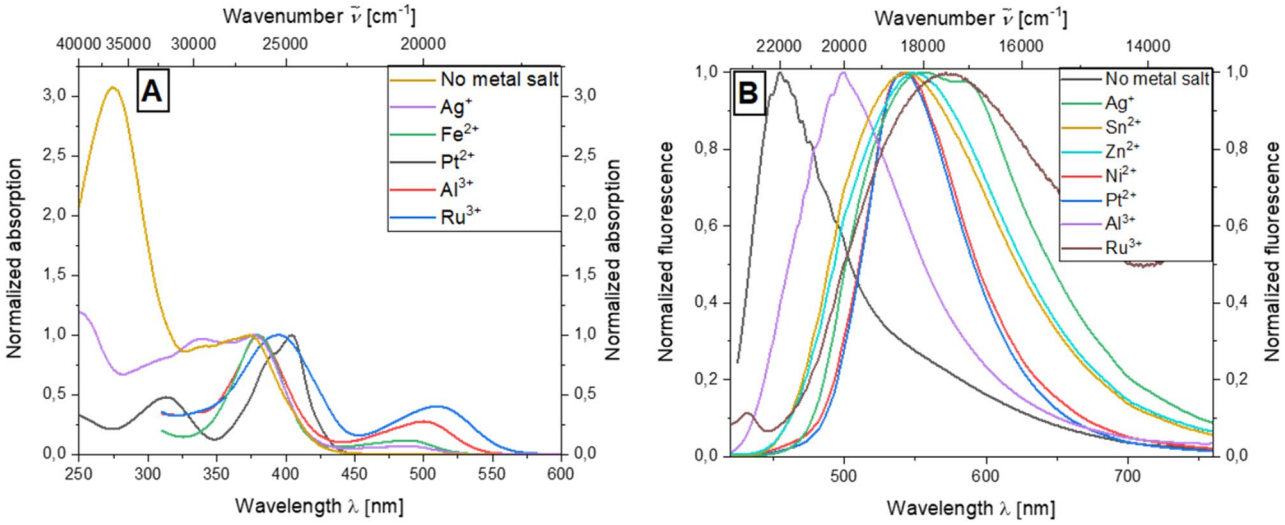

Figure 8. Absorption spectra on addition of various metal salts in ethanol (c(**5c**) = 10^{-5} M, $c(M^+) = 10^{-5}$ M, T = 298 K) (**A**) and emission spectra of compound **5c** on addition of various metal salts in ethanol (c(**5c**) = 10^{-7} M, $c(M^+) = 10^{-7}$ M, T = 298 K, λ_{exc} = 404 nm).

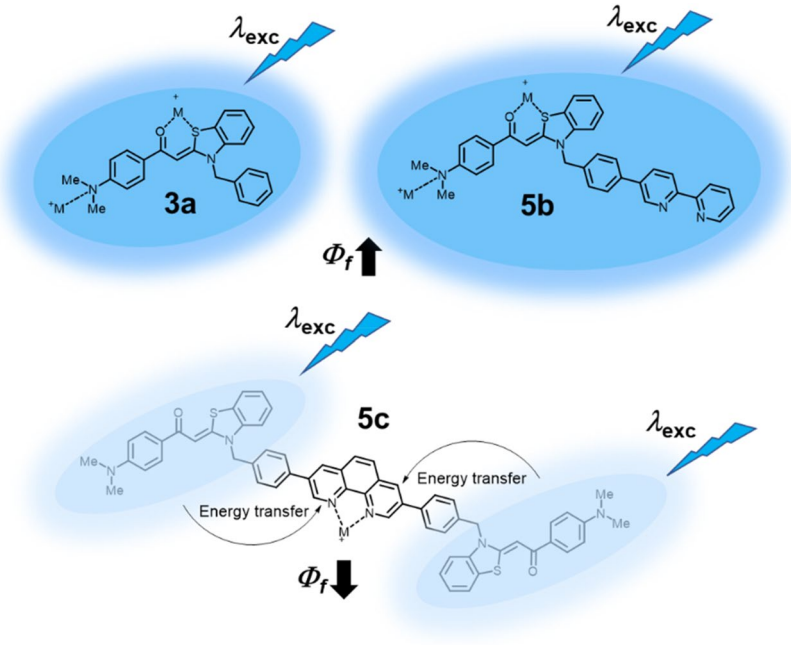

Figure 9. Potential explanatory approach to rationalize the emission enhancement of **3a** and **5a** and the quenching of the emission of **5c** in the presence of metal ions.

the emissive dimethylamino aroyl-*S*,*N*-ketene acetals to the dark, non-emissive phenanthroline-metal complex can occur (Fig. 9, bottom)[76,77].

Conclusion

In summary, bi-, multi- and single aroyl-*S*,*N*-ketene acetals were readily synthesized in mostly very good to excellent yields. Aside from typical AIE properties, these dyes exhibit pronounced complexometric behavior. Ruthenium, iron and gold cations form complexes with the investigated dyes as seen by photospectrometry. For most of the compounds, the dimethylamino substituent or the carbonyl oxygen and the sulfur of the benzothiazole are most likely sites of complexation resulting in a significant increase of quantum yield. In case of dimethylamino aroyl-*S*,*N*-ketene acetals and Au^{+}-ions, the fluorescence quantum yield is nearly tripled upon complexation. Similar trends were also observed for iron and ruthenium ions and in case of dimethylamino aroyl-*S*,*N*-ketene acetal bipyridine bichromophores. In contrast, for the 1,10-phenanthroline bridged trichromophore, the quantum yield drops presumably due to a dark state of the complexed 1,10-phenanthroline unit. For most metal ion-dye combinations, only weakly coordinating complexes could be observed by spectroscopy, only for a phenanthroline aroyl-*S*,*N*-ketene acetal multichromophore in combination with Fe^{3+}-ions, the formation of a strongly coordinating complex could be observed. In addition, even if no stable complexes are formed, the change of the emission color in the presence of different metal ions can be exploited for metal ion sensing. Future works are directed to address metal complexation for ion sensing and fishing, as well as to form more stable complexes.

Methods

The used chemicals which have not been synthesized were purchased at Acros Organics BVBA, Alfa Aeser GmbH & Co KG, Fluorochem Ltd., J&K Scientific Ltd., Merck KGaA, Macherey–Nagel GmbH & Co. KG, Sigma-Aldrich Chemie GmbH and VWR and have been used without further purification. The melting points have been measured with Melting Point B-540 of the company Büchi according to the protocol by *Kofler*[82]. All NMR and mass spectrometry experiments have been performed by the Heinrich Heine University Center of Molecular Structure Analytics (HHUCeMSA). ^{1}H, ^{13}C and DEPT 135-spectra have been measured at 298 K on an Avance III—300 and an Avance III—600 of the company Bruker. EI mass spectra have been measured with Triple Quadrupol spectrometer TSQ 7000 of the company Finnigan MAT. MALDI spectra have been measured with a MALDI/TOF UltrafleXtreme of the company Bruker Daltronik. IR spectra were recorded with neat compounds under attenuated total reflection (ATR) with IRAffinity-1 of the company Shimadzu. The elementary analyses have been measured with Perkin Elmer Series II Analyser 2400 or Vario Micro Cube of the company Analysensysteme GmbH. UV/Vis spectra of the dye solutions were measured with a Lambda 19 spectrometer from Perkin Elmer. The emission spectra of the dye solutions and the solid compounds were recorded with a Hitachi F-7000 spectrofluorometer using the emission correction curve provided by the instrument manufacturer. Emission spectra were not corrected for the wavelength-dependent spectral responsivity of the fluorometer. All solution spectra were recorded with dyes dissolved in spectroscopic grade solvents at 298 K using 1 $cm-_{quat}z$ cuvettes from Hellma GmbH. The molar extinction coefficients of dye solutions of known dye concentration were determined by five-point regression line.

For aggregation studies, samples of the aroyl-*S*,*N*-ketene acetals were dissolved in various mixtures of organic solvents and water with water contents ranging from 0 to 99%, with ethanol/water mixtures giving the clearest results, which are discussed in detail below. Furthermore, solvent mixtures of cyclohexane and dichloromethane were also tested, but no aggregate formation was observed. A stock solution of the respective chromophore was prepared in ethanol. A defined amount of this stock solution was taken, and the corresponding amount of ethanol was first placed in a 10 mL volumetric flask before the corresponding amount of water was added. To exclude aging and coagulation processes of the formed aggregates as far as possible, all solutions were first treated in an ultrasonic bath for 5 min before the emission and absorption spectra were recorded starting with the solutions of the highest water content. Selected aggregate solutions were stored for investigation of aggregate stability over time for subsequent measurements at defined time points. For the photographs of the aggregate solutions, the corresponding measurement solutions were used directly.

Data availability

All data generated or analyzed during this study are included in this published article and its supplementary information files. Experimental details of all synthesized derivatives and the respective spectroscopic and analytic data, spectra (^{1}H and ^{13}C NMR spectra, absorption and emission spectra, titration experiments) and photographs, see the accompanying Supporting Information. The datasets used and/or analyzed during the current study are available from the corresponding author on reasonable request.

Received: 7 February 2024; Accepted: 13 May 2024
Published online: 31 May 2024

References

1. Dalmieda, J. & Kruse, P. Metal cation detection in drinking water. *Sensors* **19**, 5134. https://doi.org/10.3390/s19235134 (2019).
2. Gupta, V., Ali, I. & Aboul-Enein, H. Y. Metal ions speciation in the environment: Distribution, toxicities and analyses. *Dev. Environ. Sci.* **5**, 33–56. https://doi.org/10.1016/S1474-8177(07)05003-6 (2007).
3. Zoroddu, M. A. *et al.* The essential metals for humans: A brief overview. *J. Inorg. Biochem.* **195**, 120–129. https://doi.org/10.1016/j.jinorgbio.2019.03.013 (2019).
4. Fraga, C. G. Relevance, essentiality and toxicity of trace elements in human health. *Mol. Asp. Med.* **26**, 235–244. https://doi.org/10.1016/j.mam.2005.07.013 (2005).
5. Mudgal, V., Madaan, N., Mudgal, A., Singh, R. & Mishra, S. Effect of toxic metals on human health. *Open Nutraceuticals* https://doi.org/10.2174/1876396001003010009 4 (2010).
6. Kozlowski, H., Kolkowska, P., Watly, J., Krzywoszynska, K. & Potocki, S. General aspects of metal toxicity. *Curr. Med. Chem.* **21**, 3721–3740. https://doi.org/10.2174/09298673216614071609383 8 (2014).
7. Crisponi, G. & Nurchi, V. M. Metal ion toxicity. *Encyclopedia of Inorganic and Bioinorganic Chemistry*, 1–14. https://doi.org/10.1002/9781119951438.eibc0126.pub2 (2011).
8. Stohs, S. J. & Bagchi, D. Oxidative mechanisms in the toxicity metal ions. *Free Radic. Biol. Med.* **18**, 321–336. https://doi.org/10.1016/0891-5849(94)00159-H (1995).
9. Peana, M. *et al.* Metal toxicity and speciation: A review. *Curr. Med. Chem.* **28**, 7190–7208. https://doi.org/10.2174/0929867328666210324161205 (2021).
10. Moulis, J.-M. Cellular mechanisms of cadmium toxicity related to the homeostasis of essential metals. *Biometals* **23**, 877–896. https://doi.org/10.1007/s10534-010-9336-y (2010).
11. Malik, L. A., Bashir, A., Qureashi, A. & Pandith, A. H. Detection and removal of heavy metal ions: a review. *Environ. Chem. Lett.* **17**, 1495–1521. https://doi.org/10.1007/s10311-019-00891-z (2019).
12. Zheng, X., Cheng, W., Ji, C., Zhang, J. & Yin, M. Detection of metal ions in biological systems: A review. *Rev. Anal. Chem.* **39**, 231–246. https://doi.org/10.1515/revac-2020-0118 (2020).
13. Dutta, M. & Das, D. Recent developments in fluorescent sensors for trace-level determination of toxic-metal ions. *Trends Anal. Chem.* **32**, 113–132. https://doi.org/10.1016/j.trac.2011.08.010 (2012).
14. Oehme, I. & Wolfbeis, O. S. Optical sensors for determination of heavy metal ions. *Microchim. Acta* **126**, 177–192. https://doi.org/10.1007/bf01242319 (1997).
15. Bansod, B., Kumar, T., Thakur, R., Rana, S. & Singh, I. A review on various electrochemical techniques for heavy metal ions detection with different sensing platforms. *Biosens. Bioelectron.* **94**, 443–455. https://doi.org/10.1016/j.bios.2017.03.031 (2017).
16. Nigam, A., Sharma, N., Tripathy, S. & Kumar, M. Development of semiconductor based heavy metal ion sensors for water analysis: A review. *Sens. Actuators A: Phys.* **330**, 112879. https://doi.org/10.1016/j.sna.2021.112879 (2021).
17. Dai, X., Wu, S. & Li, S. Progress on electrochemical sensors for the determination of heavy metal ions from contaminated water. *J. Chin. Adv. Mater. Soc.* **6**, 91–111. https://doi.org/10.1080/22243682.2018.1425904 (2018).
18. Hu, T., Lai, Q., Fan, W., Zhang, Y. & Liu, Z. Advances in portable heavy metal ion sensors. *Sensors* **23**, 4125. https://doi.org/10.3390/s23084125 (2023).
19. Yu, L. *et al.* Nanomaterials-based ion-imprinted electrochemical sensors for heavy metal ions detection: A review. *Biosensors* **12**, 1096. https://doi.org/10.3390/bios12121096 (2022).
20. Sharma, M. D., Rayalu, S. S., Kolev, S. D. & Krupadam, R. J. Graphene/fluorescein dye-based sensor for detecting As (III) in drinking water. *Sci. Rep.* **11**, 17321. https://doi.org/10.1038/s41598-021-96968-3 (2021).
21. Rout, B. A miniaturized therapeutic chromophore for multiple metal pollutant sensing, pathological metal diagnosis and logical computing. *Sci. Rep.* **6**, 27115. https://doi.org/10.1038/srep27115 (2016).
22. Ghosh, P. & Roy, P. Structure–metal ion selectivity of rhodamine-based chemosensors. *Chem. Commun.* **59**, 5174–5200. https://doi.org/10.1039/d3cc00651d (2023).
23. Sareen, D., Kaur, P. & Singh, K. Strategies in detection of metal ions using dyes. *Coord. Chem. Rev.* **265**, 125–154. https://doi.org/10.1016/j.ccr.2014.01.015 (2014).
24. Carter, K. P., Young, A. M. & Palmer, A. E. Fluorescent sensors for measuring metal ions in living systems. *Chem. Rev.* **114**, 4564–4601. https://doi.org/10.1021/cr400546e (2014).
25. Kaur, B., Kaur, N. & Kumar, S. Colorimetric metal ion sensors—A comprehensive review of the years 2011–2016. *Coord. Chem. Rev.* **358**, 13–69. https://doi.org/10.1016/j.ccr.2017.12.002 (2018).
26. De Acha, N., Elosúa, C., Corres, J. M. & Arregui, F. J. Fluorescent sensors for the detection of heavy metal ions in aqueous media. *Sensors* **19**, 599. https://doi.org/10.3390/s19030599 (2019).
27. Kaur, N. & Kumar, S. Colorimetric metal ion sensors. *Tetrahedron* **67**, 9233–9264. https://doi.org/10.1016/j.tet.2011.09.003 (2011).

28. Gul, Z., Khan, S. & Khan, E. Organic molecules containing N, S and O heteroatoms as sensors for the detection of Hg (II) ion; coordination and efficiency toward detection. *Crit. Rev. Anal. Chem.* https://doi.org/10.1080/10408347.2022.2121600 (2022).
29. Ríos, M.-C., Bravo, N.-F., Sánchez, C.-C. & Portilla, J. Chemosensors based on N-heterocyclic dyes: Advances in sensing highly toxic ions such as CN− and Hg 2+. *RSC Adv.* **11**, 34206–34234. https://doi.org/10.1039/d1ra06567j (2021).
30. Antina, E. V., Bumagina, N. A., V'yugin, A. I. & Solomonov, A. V. Fluorescent indicators of metal ions based on dipyrro methene platform. *Dyes Pigment.* **136**, 368–381. https://doi.org/10.1016/j.dyepig.2016.08.070 (2017).
31. Iftikhar, R. *et al.* Small organic molecules as fluorescent sensors for the detection of highly toxic heavy metal cations in portable water. *J. Environ. Chem. Eng.* **11**, 109030. https://doi.org/10.1016/j.jece.2022.109030 (2023).
32. Hancock, R. D. The pyridyl group in ligand design for selective metal ion complexation and sensing. *Chem. Soc. Rev.* **42**, 1500–1524. https://doi.org/10.1039/c2cs35224a (2013).
33. Ashraf, A. *et al.* Naphthyridine derived colorimetric and fluorescent turn off sensors for Ni2+ in aqueous media. *Sci. Rep.* **11**, 19242. https://doi.org/10.1038/s41598-021-98400-2 (2021).
34. Razavi, S. A. A. & Morsali, A. Metal ion detection using luminescent-MOFs: Principles, strategies and roadmap. *Coord. Chem. Rev.* **415**, 213299. https://doi.org/10.1016/j.ccr.2020.213299 (2020).
35. Yan, D., Tang, Y., Lin, H. & Wang, D. Tunable two-color luminescence and host–guest energy transfer of fluorescent chromophores encapsulated in metal-organic frameworks. *Sci. Rep.* **4**, 4337. https://doi.org/10.1038/srep04337 (2014).
36. Shamim, M. A., Zia, H., Zeeshan, M., Khan, M. Y. & Shahid, M. Metal organic frameworks (MOFs) as a cutting-edge tool for the selective detection and rapid removal of heavy metal ions from water: Recent progress. *J. Environ. Chem. Eng.* **10**, 106991. https://doi.org/10.1016/j.jece.2021.106991 (2022).
37. Săcărescu, L., Chibac-Scutaru, A.-L., Roman, G., Săcărescu, G. & Simionescu, M. Selective detection of metal ions, sulfites and glutathione with fluorescent pyrazolines: A review. *Environ. Chem. Lett.* **21**, 561–596. https://doi.org/10.1007/s10311-022-01508-8 (2023).
38. Qiao, M., Ding, L. & Lv, F. Surfactant assemblies encapsulating fluorescent probes as selective and discriminative sensors for metal ions. *Coord. Chem. Rev.* **432**, 213696. https://doi.org/10.1016/j.ccr.2020.213696 (2021).
39. She, M. *et al.* Design strategy and recent progress of fluorescent probe for noble metal ions (Ag, Au, Pd, and Pt). *Coord. Chem. Rev.* **432**, 213712. https://doi.org/10.1016/j.ccr.2020.213712 (2021).
40. Rurack, K. Flipping the light switch 'ON'–the design of sensor molecules that show cation-induced fluorescence enhancement with heavy and transition metal ions. *Spectrochim. Acta A* **57**, 2161–2195. https://doi.org/10.1016/s1386-1425(01)00492-9 (2001).
41. Kaushal, S., Kaur, M., Kaur, N., Kumari, V. & Singh, P. P. Heteroatom-doped graphene as sensing materials: A mini review. *RSC Adv.* **10**, 28608–28629. https://doi.org/10.1039/d0ra04432f (2020).
42. Bogireddy, N. K. R., Rios, S. E. S. & Agarwal, V. Simple one step synthesis of dual-emissive heteroatom doped carbon dots for acetone sensing in commercial products and Cr (VI) reduction. *Chem. Eng. J.* **414**, 128830. https://doi.org/10.1016/j.cej.2021.128830 (2021).
43. Yoo, D., Park, Y., Cheon, B. & Park, M.-H. Carbon dots as an effective fluorescent sensing platform for metal ion detection. *Nanoscale Res. Lett.* **14**, 1–13. https://doi.org/10.1186/s11671-019-3088-6 (2019).
44. Li, P. & Li, S. F. Recent advances in fluorescence probes based on carbon dots for sensing and speciation of heavy metals. *Nanophotonics* **10**, 877–908. https://doi.org/10.1515/nanoph-2020-0507 (2020).
45. Biranje, A., Azmi, N., Tiwari, A. & Chaskar, A. Quantum dots based fluorescent probe for the selective detection of heavy metal ions. *J. Fluoresc.* **31**, 1241–1250. https://doi.org/10.1007/s10895-021-02755-8 (2021).
46. Devi, P., Rajput, P., Thakur, A., Kim, K.-H. & Kumar, P. Recent advances in carbon quantum dot-based sensing of heavy metals in water. *Trends Anal. Chem.* **114**, 171–195. https://doi.org/10.1016/j.trac.2019.03.003 (2019).
47. Alam, P. *et al.* AIE-based luminescence probes for metal ion detection. *Coord. Chem. Rev.* **429**, 213693. https://doi.org/10.1016/j.ccr.2020.213693 (2021).
48. Ye, F.-Y., Hu, M. & Zheng, Y.-S. Advances and challenges of metal ions sensors based on AIE effect. *Coord. Chem. Rev.* **493**, 215328. https://doi.org/10.1016/j.ccr.2023.215328 (2023).
49. Wan, H. *et al.* AIE-based fluorescent sensors for low concentration toxic ion detection in water. *J. Hazard. Mat.* **403**, 123656. https://doi.org/10.1016/j.jhazmat.2020.123656 (2021).
50. Li, Y., Zhong, H., Huang, Y. & Zhao, R. Recent advances in AIEgens for metal ion biosensing and bioimaging. *Molecules* **24**, 4593. https://doi.org/10.3390/molecules24244593 (2019).
51. Chua, M. H., Zhou, H., Zhu, Q., Tang, B. Z. & Xu, J. W. Recent advances in cation sensing using aggregation-induced emission. *Mater. Chem. Front.* **5**, 659–708. https://doi.org/10.1039/d0qm00607f (2021).
52. La, D. D., Bhosale, S. V., Jones, L. A. & Bhosale, S. V. Tetraphenylethylene-based AIE-active probes for sensing applications. *ACS Appl. Mater. Interfaces* **10**, 12189–12216. https://doi.org/10.1021/acsami.7b12320 (2017).
53. Biesen, L. & Müller, T. J. J. Aroyl-S, N-ketene acetals: Luminous renaissance of a class of heterocyclic compounds. *Chem. Eur. J.* https://doi.org/10.1002/chem.202302067 (2023).
54. Biesen, L., Nirmalananthan-Budau, N., Hoffmann, K., Resch-Genger, U. & Müller, T. J. J. Solid-state emissive aroyl-S, N-ketene acetals with tunable aggregation-induced emission characteristics. *Angew. Chem. Int. Ed.* **59**, 10037–10041. https://doi.org/10.1002/anie.201916396 (2020).
55. Biesen, L., Hartmann, Y. & Müller, T. J. J. Alkynylated and triazole-linked aroyl-S, N-ketene acetals—One-pot synthesis of solid-state emissive dyes with aggregation-induced enhanced emission characteristics. *Sci. Rep.* **13**, 14399. https://doi.org/10.1038/s41598-023-41146-w (2023).
56. Biesen, L., Krenzer, J., Nirmalananthan-Budau, N., Resch-Genger, U. & Müller, T. J. J. Asymmetrically bridged aroyl-S, N-ketene acetal-based multichromophores with aggregation-induced tunable emission. *Chem. Sci.* **13**, 5374–5381. https://doi.org/10.1039/d2sc00415a (2022).
57. Biesen, L. *et al.* Communication of bichromophore emission upon aggregation–aroyl-S, N-ketene acetals as multifunctional sensor merocyanines. *Chem. Eur. J.* **27**, 13426–13434. https://doi.org/10.1002/chem.202102052 (2021).
58. Biesen, L., Hartmann, Y. & Müller, T. J. J. Diaroyl-S, N-ketene acetals—Red-shifted solid-state and ag-gregation-induced emitters via one-pot synthesis. *Chem. Eur. J.* https://doi.org/10.1002/chem.202301908 (2023).
59. Biesen, L. & Müller, T. J. J. Solid-state emissive biphenylene bridged bisaroyl-S, N-ketene acetals as distinct aggregation-induced enhanced emitters and fluorometric probes. *Aggregate* **2**, e105. https://doi.org/10.1002/agt2.105 (2021).
60. Biesen, L. & Müller, T. J. J. Single molecule aggregation-induced dual and white-light emissive etherified aroyl-S, N-ketene acetals via one-pot synthesis. *RSC Adv.* **13**, 16867–16871. https://doi.org/10.1039/d3ra02935b (2023).
61. Wang, T., Xie, H., Liu, L. & Zhao, W.-X. N-heterocyclic carbene-palladium (II) complexes with benzoxazole or benzothiazole ligands: Synthesis, characterization, and application to Suzuki-Miyaura cross-coupling reaction. *J. Organomet. Chem.* **804**, 73–79. https://doi.org/10.1016/j.jorganchem.2015.12.039 (2016).
62. Wang, Z. *et al.* Cyclopentadienyl molybdenum (II) N, C-chelating benzothiazole-carbene complexes: synthesis, structure, and application in cyclooctene epoxidation catalysis. *Organometallics* **33**, 2457–2466. https://doi.org/10.1021/om401128z (2014).
63. Li, Q. *et al.* Luminescent copper (I) complexes bearing benzothiazole-imidazolylidene ligand with various substituents: Synthesis, photophysical properties and computational studies. *Polyhedron* **218**, 115785. https://doi.org/10.1016/j.poly.2022.115785 (2022).
64. Ye, S., Liang, Q., Li, Z., Xu, S. & Yao, C. A highly sensitive and selective naked-eye probe for detection of Fe3+ based on a 2, 5-bis [3-benzyl-2-methylbenzothiazole]-croconaine. *Tetrahedron* **73**, 1350–1357. https://doi.org/10.1016/j.tet.2017.01.049 (2017).

65. Yang, Z. *et al.* Triphenylethylene carbazole derivatives as a new class of AIE materials with strong blue light emission and high glass transition temperature. *J. Mater. Chem.* **19**, 5541–5546. https://doi.org/10.1039/B902802A (2009).
66. Kruppa, M. & Müller, T. J. J. Masuda Borylation–Suzuki coupling (MBSC) sequence: A one-pot process to access complex (hetero) biaryls. *Catalysts* **13**, 350. https://doi.org/10.3390/catal13020350 (2023).
67. Renny, J. S., Tomasevich, L. L., Tallmadge, E. H. & Collum, D. B. Method of continuous variations: Applications of job plots to the study of molecular associations in organometallic chemistry. *Angew. Chem. Int. Ed.* **52**, 11998–12013. https://doi.org/10.1002/anie.201304157 (2013).
68. Huang, C. Y. *Methods in Enzymology* Vol. 87, 509–525 (Elsevier, Amsterdam, 1982). https://doi.org/10.1016/s0076-6879(82)87029-8.
69. Rurack, K. Flipping the light switch 'On'—The design of sensor molecules that show cation-induced fluorescence enhancement with heavy and transition metal ions. *Spectrochim. Acta A Mol. Biomol. Spectrosc.* **57**, 2161–2195. https://doi.org/10.1016/S1386-1425(01)00492-9 (2001).
70. Ramachandram, B. & Samanta, A. Transition metal ion induced fluorescence enhancement of 4-(N, N-dimethylethylenediamino)-7-nitrobenz-2-oxa-1,3-diazole. *J. Phys. Chem. A* **52**, 10579–10587. https://doi.org/10.1021/jp983106d (1998).
71. Li, S., He, J. & Xu, Q.-H. Aggregation of metal-nanoparticle-induced fluorescence enhancement and its application in sensing. *ACS Omega* **5**, 41–48. https://doi.org/10.1021/acsomega.9b03560 (2020).
72. Charlier, P., Jerome, R. & Teyssie, P. Solution behavior of α, ι-(dimethylamino) polyisoprene coordinated to transition metal salts. *Macromolecules* **23**, 1831–1837. https://doi.org/10.1021/ma00208a046 (1990).
73. Yamasaki, T. *et al.* First transition metal complex of 1, 8-bis (dimethylamino) naphthalene (proton sponge). *Chem. Lett.* **33**, 928–929. https://doi.org/10.1246/cl.2004.928 (2004).
74. Grove, D., Van Koten, G., Ubbels, H., Zoet, R. & Spek, A. Organonickel (II) complexes of the tridentate monoanionic ligand o, o'-bis [(dimethylamino) methylphenyl (NCN). Syntheses and the x-ray crystal structure of the stable nickel (II) formate [Ni (NCN) O2CH]. *Organometallics* **3**, 1003–1009. https://doi.org/10.1021/om00085a007 (1984).
75. Liu, Z., He, W. & Guo, Z. Metal coordination in photoluminescent sensing. *Chem. Soc. Rev.* **42**, 1568–1600. https://doi.org/10.1039/c2cs35363f (2013).
76. Sammes, P. G. & Yahioglu, G. 1, 10-Phenanthroline: A versatile ligand. *Chem. Soc. Rev.* **23**, 327–334. https://doi.org/10.1039/cs9942300327 (1994).
77. Bencini, A. & Lippolis, V. 1, 10-Phenanthroline: A versatile building block for the construction of ligands for various purposes. *Coord. Chem. Rev.* **254**, 2096–2180. https://doi.org/10.1016/j.ccr.2010.04.008 (2010).
78. Fabbrizzi, L., Licchelli, M., Pallavicini, P., Sacchi, D. & Taglietti, A. Sensing of transition metals through fluorescence quenching or enhancement. A review. *Analyst* **121**, 1763–1768. https://doi.org/10.1039/AN9962101763 (1996).
79. Varnes, A. W., Dodson, R. B. & Wehry, E. E. Wehry, Interactions of transition-metal ions with photoexcited states of flavines. Fluorescence quenching studies. *J. Am. Chem. Soc.* **94**, 946–950. https://doi.org/10.1021/ja00758a037 (1972).
80. Accorsi, G., Listorti, A., Yoosaf, K. & Armaroli, N. 1,10-Phenanthrolines: Versatile building blocks for luminescent molecules, materials and metal complexes. *Chem. Soc. Rev.* **38**, 1690–1700. https://doi.org/10.1039/B806408N (2009).
81. Alreja, P. & Kaur, N. Recent advances in 1,10-phenanthroline ligands for chemosensing of cations and anions, Recent advances in 1,10-phenanthroline ligands for chemosensing of cations and anions. *RSC Adv.* **6**, 23169–23217. https://doi.org/10.1039/C6RA00150E (2016).
82. Kuhnert-Brandstatter, Identifizierung organischer Substanzen nach L. Kofler. M. *Sci. Pharm.* **34**, 147–166 (1966).

Acknowledgements

The authors cordially thank the Fonds der Chemischen Industrie and the Deutsche Forschungsgemeinschaft (Mu 1088/9-1) and a Walter Benjamin scholarship of the Deutsche Forschungsgemeinschaft (Project No. 527594635) for financial support. We also thank the CeMSA@HHU (Center for Molecular and Structural Analytics @ Heinrich Heine University) for recording mass-spectrometric and the NMR spectroscopic data.

Author contributions

The first draft of this manuscript was written by L.B., review, editing, funding acquisition, and project administration was done by T.J.J.M. All authors have commented and given approval to the final version of the manuscript.

Funding

Open Access funding enabled and organized by Projekt DEAL.

Competing interests

The authors declare no competing interests.

Additional information

Supplementary Information The online version contains supplementary material available at https://doi.org/10.1038/s41598-024-62100-4.

Correspondence and requests for materials should be addressed to T.J.J.M.